MAX-PLANCK-INSTITUT
FÜR METEOROLOGIE

Implementation of riverine organic carbon transport into the land surface model JSBACH

- Technical Note -

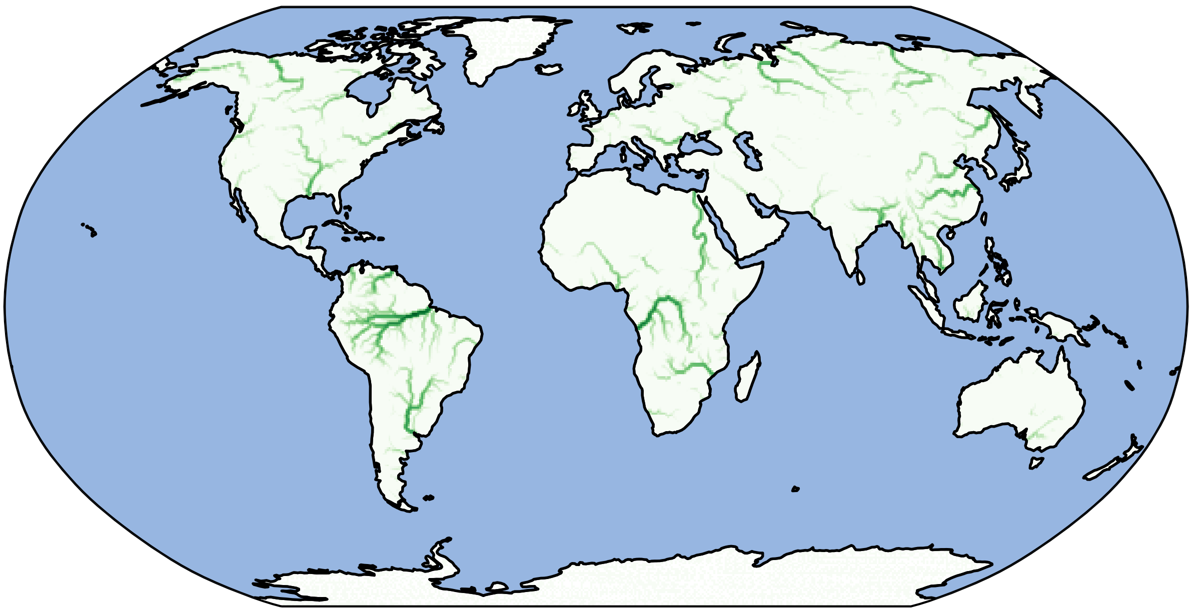

Swati Gehlot, Thomas Riddick,
Stefan Hagemann, Victor Brovkin

Hamburg 2024

Berichte zur Erdsystemforschung
Reports on Earth System Science

284
2024

Hinweis

Die Berichte zur Erdsystemforschung werden vom Max-Planck-Institut für Meteorologie in Hamburg in unregelmäßiger Abfolge herausgegeben.

Sie enthalten wissenschaftliche und technische Beiträge, inklusive Dissertationen.

Die Beiträge geben nicht notwendigerweise die Auffassung des Instituts wieder.

Die "Berichte zur Erdsystemforschung" führen die vorherigen Reihen "Reports" und "Examensarbeiten" weiter.

Anschrift / Address

Max-Planck-Institut für Meteorologie
Bundesstrasse 53
20146 Hamburg
Deutschland

Tel./Phone: +49 (0)40 4 11 73 - 0
Fax: +49 (0)40 4 11 73 - 298

name.surname@mpimet.mpg.de
www.mpimet.mpg.de

Notice

The Reports on Earth System Science are published by the Max Planck Institute for Meteorology in Hamburg. They appear in irregular intervals.

They contain scientific and technical contributions, including PhD theses.

The Reports do not necessarily reflect the opinion of the Institute.

The "Reports on Earth System Science" continue the former "Reports" and "Examensarbeiten" of the Max Planck Institute.

Layout

Bettina Diallo and Norbert P. Noreiks
Communication

Copyright

Implementation of riverine organic carbon transport into the land surface model JSBACH

- Technical Note -

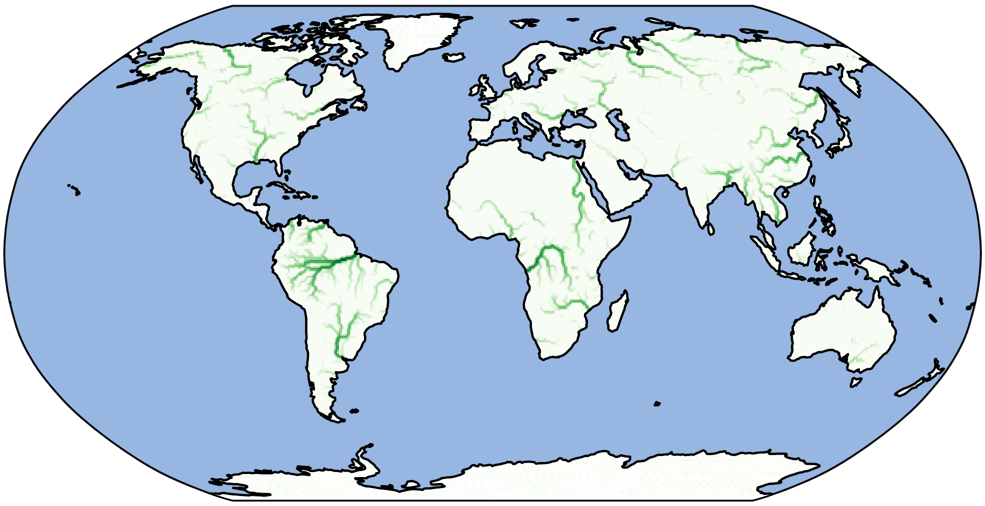

Swati Gehlot, Thomas Riddick,
Stefan Hagemann, Victor Brovkin

Hamburg 2024

Swati Gehlot[1,2*], Thomas Riddick[1*],
Stefan Hagemann[3], Victor Brovkin[1,4]

[1] Max-Planck-Institut für Meteorologie, Hamburg
[2] DKRZ, Hamburg
[3] Institut für Küstensysteme, Helmholz-Zentrum Hereon, Geesthacht
[4] Centrum für Erdsystemforschung und Nachhaltigkeit (CEN), Universität Hamburg
[*] Diese beiden Autoren haben gleichermaßen zu dieser Arbeit beigetragen.

Berichte zur Erdsystemforschung / Max-Planck-Institut für Meteorologie 284
Reports on Earth System Science / Max Planck Institute for Meteorology 2024

ISSN 1614-1199 - doi: 10.17617/2.3602778

Abstract

The lateral transport of terrestrial carbon (C) to the ocean via river networks is an important component of the carbon cycle. This process is currently neglected in many Earth System Models (ESMs) leading to an overestimation of the terrestrial C sink.

In the newly developed riverine carbon transport scheme for the land surface component JSBACH of the Max Planck Institute for Me-teorology ESM (MPI-ESM), the source and subsequent transport of organic carbon from the soil to the river systems via surface runoff is calculated. The flow properties of dissolved organic carbon (DOC) are simulated in a way analogous to the lateral transport of water over land based on a set of predefined river directions and rates of flow. The water-soluble soil carbon pool is interpolated from the coarser JSBACH grid to the finer Hydrological Discharge (HD) model grid on which lateral hydrological transport is better represented. As the water-soluble carbon is degradable, we simulated its decay over time using near surface soil temperature as a proxy for water temperature.

For comparison with observations, JSBACH is driven by a mete-orological forcing dataset based on re-analysis and observations. We evaluated the model using sensitivity experiments with different frac-tions of carbon transfer and decay rates. Our approach reproduces the main features of the seasonality of riverine DOC flux.

1 Introduction

The interaction of soil with land surface hydrology and the subsequent discharge of water through the terrestrial drainage network (rivers and streams) plays an important role in land to ocean carbon transfer. This land to ocean carbon transport through the terrestrial drainage network, as well as vertical flux transitions (as greenhouse gases), during this transport are acknowledged in the 6th Assessment Report of the Intergovernmental Panel on Climate Change (IPCC) [*Canadell et. al.*, 2021]. Nonetheless, current state-of-the-art Earth System Models (ESMs) usually consider only the vertical gas exchanges between the atmosphere and land/ocean and omit the lateral carbon fluxes carried by the network of rivers to the ocean. This exclusion leads to an overestimation of soil carbon sequestration and thus the terrestrial carbon sink [*Jackson et. al.*, 2002]. Ideally ESMs need to include the effect of lateral carbon and nutrients transfer and its subsequent alteration during riverine transit in order to provide a better representation of the global carbon cycle [*Lacroix et. al.*, 2021]. This quantification of land-atmosphere exchange of global C is a useful component of models used to assess future projections of atmospheric CO_2 concentrations and global carbon stocks [*Battin et. al.*, 2009]. The transfer of carbon flux from soil to the rivers in form of dissolved organic carbon is estimated to be 37 % of the total global riverine carbon export via land to the ocean [*Meybeck*, 1993]. Organic carbon enters rivers throughout their catchment area by drainage and by direct deposition from adjacent terrestrial ecosystems along with autocthonous carbon fixation [*Schlesinger and Melack*, 1981].

Riverine dissolved organic carbon (DOC) originates from a variety of sources, primarily resulting from root exudates (or plant residues) and their subsequent interaction with soil as a medium [*Hansell et. al.*, 2004; *Li et. al.*, 2017]. DOC originating from the soil can be produced in-situ with or without the addition of advective fluxes within the soil water. This DOC is leached to the river network via the surface runoff and sub-surface drainage. The fate of this DOC in terms of the proportion transported downstream by the river network, the proportion evaded in form of CO_2, and the proportion that undergoes physical sedimentation are key considerations in understanding the terrestrial-hydrological link within the global carbon cycle [*Cole et. al.*, 2007; *Battin et. al.*, 2009].

The purpose of this report is to address this rather small, but not insignificant and poorly studied component of the carbon cycle connecting the soil carbon to the oceans via the network of rivers and streams across the globe. We aim to estimate the global riverine DOC flux from organic carbon leached from the soil to the river networks.

2 Methods

A block diagram with an overview of the main routines of our DOC model in pseudo-code is shown in Figure 1. The following subsections provide a brief description of the existing model components used in the new riverine DOC scheme (Sections 2.1 and 2.2) followed by description of the new components added for the scheme itself (Sections 2.3, 2.4 and 2.5) and of the forcing and initialisation procedure used (Section 2.6).

2.1 JSBACH Land surface model

We use a version of the JSBACH 3 [*Reick et. al.*, 2021] land surface model which includes a soil carbon model [*Goll et. al.*, 2015] and a five-layer soil hydrology scheme [*Hagemann and Stacke*, 2015; *Mauritsen et. al.*, 2019]. Additionally included in the version of JSBACH used is a representation of permafrost processes [*Ekici et. al.*, 2014].

The Yasso soil carbon scheme implemented within JSBACH is based on the litter-bag experiments for soil carbon decomposition measurements [*Tuomi et. al.*, 2008; *Thum et. al.*, 2011]. The different types of soil organic carbon are classified based on their solubility parameters. The litter (woody and green) is distinguished based on its decomposition solubility in (1) Acid, (2) water and (3) Ethanol, alongside a (4) non-soluble component, for both the sub-categories of above-ground and below-ground for each vegetation tile. Each of these compound groups has a specific decomposition rate, for example the woody litter decomposition rate is lower than that of green litter. In addition, the humus soil carbon pool (also in two categories) is distinguished by its longer decomposition time scales.

2.2 Hydrological Discharge (HD) model

The lateral freshwater hydrological fluxes within JSBACH are treated by the Hydrological Discharge (HD) model [*Hagemann and Dümenil*, 1998; *Hagemann and Dümenil-Gates*, 2001]. Although the HD model is integrated within JSBACH, it can also be run independently as a standalone model (HD-offline). The core concept of HD model is to use the aggregation of surface flow and the sub-surface flow to calculate the routed river flow discharge (channelled flow, direction based). These three flow components in each grid cell ($0.5° \times 0.5°$) are computed within the HD model, namely the overland flow (representing surface runoff), base flow (drainage or slow moving sub-surface flow) and river flow (routed river or channelled flow). All three components of the flow from a cell are directed to one of the cell's eight direct neighbours.

The surface runoff as well as the drainage of each JSBACH grid cell (at T63 resolution) is collected and interpolated to the 0.5° resolution and added to the overland flow and base flow respectively. The overland flow and base flow are each modeled by a single linear reservoir for each grid cell. The sum of overland flow, base flow and inflow from other neighbouring grid-cells contribute to the river flow which is modelled through a cascade of n linear reservoirs (n is 5 without lakes and 1 with lakes). A cascade of linear reservoirs in each cell is necessary to accurately simulate the rate at which the water passes through the cell and the quantity of water stored in the cell (retention characteristics), utilizing model parameters like slope within a grid box, the grid box length, the lake area, and the wetland fraction of the grid cell.

The river flow out of a given cell as a function of time, $Q(t)$, measured in general flow units such as $\mathrm{m}^3\mathrm{day}^{-1}$, is modelled as:

$$Q(t) = \frac{S(t)}{k} \tag{1}$$

where $S(t)$ is the river water reservoir volume, m^3, as a function of time and k is the retention coefficient of the reservoir, given in days.

The retention coefficient k_r of particular river reservoir $r = 1, ..., n$, days, is calculated for each grid cell as:

$$k_r = k_{ref} \cdot \frac{\Delta x}{s^{0.1}} \tag{2}$$

where k_{ref} is a reference retention value, day$\cdot\, m^{-1}$, Δx is the distance between the centers of given cell and the next cell downstream of it and slope, s, is calculated as $s = \Delta h / \Delta x$ where Δh is the height difference between the cell and the next downstream cell, both in meters. This calculation is modified when lakes or wetlands are present in the cell.

The overland and base flows are calculated using similar equations to equation 1, but their retention coefficients are calculated differently.

2.3 Leaching of Carbon from YASSO Carbon pools

In this report we consider two variants of our model; these differ in the selection of carbon pools that contribute to the leaching of carbon into the hydrological system to further propagate as riverine DOC. These two variants are:

Variant A Contributions from the YASSO water soluble pool only.

Variant B Contributions from all YASSO pools.

Both variants are useful to test the dependency of transported carbon on the involvement of different pools. During each JSBACH model time step, a fraction f_{leach}, of the carbon is removed from each contributing YASSO carbon pool, accumulated, and provided to the riverine DOC transport scheme (see next section) at the next HD model time-step. This process represents the leaching of carbon out of the soil into the river network. For each contributing carbon pool the fraction of the pool leached at each time-step is given by:

$$f_{\text{leach}} = f_0 \times s_{\text{runoff}} \tag{3}$$

where f_0 is a global constant and:

$$s_{\text{runoff}} = \min(1, \frac{\mathrm{R}}{\max(10^{-13}, R_{\text{20-year-max-runoff}})}) \tag{4}$$

where runoff, R, and 20 year maximum runoff, $R_{\text{20-year-max-runoff}}$, are measured in $\mathrm{m^3 day^{-1}}$. Alternatively, a running mean of the runoff could be used instead of 20-year maximum runoff.

The contribution of carbon transported via drainage or sub surface flow is considered to be rather insignificant due to the influence of sedimentation processes, filtering and local effects. Hence, the C leaching via subsurface drainage is currently neglected in our approach.

To represent the transport of vegetation litter (carbon pools), a fraction of above ground litter pool, f_{litter}, is removed from the litter pool and accumulated for addition to the riverine DOC transport scheme alongside the contributions from the other pools at the next HD model time-step (day). This fraction is given by:

$$f_{\text{litter}} = f_{\text{leach}}. \tag{5}$$

2.4 Carbon transport scheme for riverine transport of carbon pools

We model the lateral transport of DOC by replicating the HD model infrastructure where the flux of water is substituted for a flux of terrestrial carbon. The water soluble component of the YASSO soil carbon pool (above and below the ground surface) is used as a primary input to this riverine carbon transport scheme (in variant B the water insoluble component(s) of the YASSO soil carbon pool are also used as primary input). The fluxes from the above ground and below ground water soluble carbon pools enter the equivalent of the surface runoff (and for variant B also the fluxes from water insoluble carbon pools). The surface carbon flux propagates one cell downstream and then becomes the carbon flow in the channelled river network. The riverine carbon flow is modelled analogously to the river discharge in the HD model [*Hagemann and Dümenil*, 1998] and based on the same flow properties (retention time, slope gradient between grid cells, number of linear reservoirs (5 in the current case)).

As tested in the early model evaluation of this study (not shown in this report), the authors found out that the C flux transport via subsurface leaching is quantitatively negligible, therefore only the overland flow C flux is relevant for DOC transport in our scheme. This could be improved in later model developments and perhaps with more rigorous testing with different C fractions as input to the scheme.

2.5 Implementation of temperature-dependent decay for transport of riverine carbon flux

The decay and evasion of DOC in rivers during the process of lateral transport is driven by a combination of photo-chemical consumption [*Cory et. al.*, 2014] and microbial consumption [*Amon and Benner*, 1996] and also depends on the exact nature of the organic carbon being transported [*Textor et. al.*, 2019]. Here we choose to model it using a very simple representation based on temperature dependence following very similar approaches of [*Li et. al.*, 2019; *Tian et. al.*, 2015].

We represent the decomposition and evasion of dissolved organic carbon (DOC) in rivers to the atmosphere by a basic exponential decay formulation using a $Q10$ based temperature dependence. The mass of carbon after decay, m_{t_1}, in the riverine DOC reservoirs is calculated according to the equation:

$$m_{t_1} = e^{-\lambda \Delta t} \cdot m_{t0} \tag{6}$$

where Δt is the time-step, day, m_{t0} the prior mass of DOC and the rate of decay λ, day^{-1}, is given by:

$$\lambda = \lambda_{T_{ref}} \cdot Q10^{(T-T_{ref})/T_{base}} \tag{7}$$

Here $\lambda_{T_{ref}}$, day^{-1}, and $Q10$ are empirically derived fixed global constants and T, K, is the mean temperature of the first two surface layers of the nearest

JSBACH3 grid cell on the Gaussian grid. $T_{ref} = 293.15K$ and $T_{base} = 10K$ are constants.

This decay is applied to all DOC in rivers at each HD model time-step (every day). Carbon release to the atmosphere is currently simply removed from the model. In the case of emission-driven simulations, this flux should be added to the atmospheric component of MPI-ESM as a carbon flux from the land surface to the atmosphere (not implemented in the current JSBACH3 code).

2.6 Initialization of HD model and input from JSBACH soil carbon

Soil carbon decomposition in the Yasso model depends on the air temperature and precipitation (and on simulated soil temperature and moisture in permafrost regions), making it crucial to use observed forcing data for model evaluation. Here, we use the Global Soil Wetness Project Phase 3 (GWSP3; [*Dirmeyer et. al.*, 2006; *Kim. H.*, 2017]) dataset that comprises 3-hourly data at 0.5° resolution from 1901-2014. To generate the GSWP3 dataset, the 20th Century Reanalysis (20CR; [*Compo et. al.*, 2011] was first dynamically downscaled onto the T248 (0.5°) grid using a spectral nudging technique [*Yoshimura and Kanamitsu*, 2008] in a Global Spectral Model (GSM). Then observation based bias correction procedures were applied to the downscaled data to yield daily time series.

We conducted various sensitivity simulations for the historical period (1901-2014) that were preceded by a spin-up of several thousand years (with the added permafrost component active) in order to allow the Yasso soil carbon pools to reach equilibrium. The model was then first run for the period from 1901-1950 so that the HD model reservoirs could stabilize. For the evaluation, the model output was averaged over a 30-year period to yield a representative monthly climatology. In order to evaluate the model based only on soil carbon and hydrology effects, the associated JSBACH dynamic vegetation model, wildfire model, land-use changes as well as nitrogen cycle were deactivated throughout the model runs (including during the spin-up and HD model stabilization).

3 Model sensitivity framework

The developed carbon transport model is tested based on the sensitivity to changes in spatial resolution, carbon pools available for leaching, and parameters controlling decomposition rate. The experiment runs are carried out in two sets - sets A and B corresponding to the two model variants A and B respectively - each with a series of individual tests conducted for a range of values of f_0 and a range of decay rate λ values,day^{-1}. As described above, model variants (and hence test sets) A and B use two different implementations of leaching of soil carbon. The difference between them is which Yasso carbon pools contribute to the soil carbon flux to the HD model. In variant (and test set) A only the Yasso water soluble carbon pools contribute to the riverine carbon (Table 1) while in variant (and test set) B all Yasso pools (AWEN) contribute to the riverine carbon (using the same test set as in variant A).

Table 1: Experiment list for model variant set A: only Yasso water soluble carbon pools contributing to the riverine carbon with corresponding variation for C percentage f_0, and $\lambda_{T_{ref}}$, day^{-1}. Similar test runs were performed for model variant set B consisting of all Yasso AWEN pools contribution to riverine DOC.

Experiment name	**Yasso water soluble Pools f_0**	$\lambda_{T_{ref}}$, **day^{-1}**
Test 01	0.1%	0.0
Test 02	0.1%	0.046
Test 03	0.1%	0.172
Test 04	1.0%	0.0
Test 05	1.0%	0.046
Test 06	1.0%	0.172

3.1 Model Sensitivity to Q10 and λ_{Tref}

We tested the sensitivity of our model to Q10 by running a set of simulations using model variant B (results for variant A displayed a similar scaling), f_0 of 0.1% and a standard λ_{Tref} of 0.046 day^{-1} and T_{ref} of 293.15 K. Table 2 shows the yearly total riverine DOC reaching the ocean for a plausible range of Q10 values. The total riverine DOC flux to the ocean increases with Q10, this behavior is expected for rivers where the water temperature is generally less than T_{ref}. The DOC flux to the ocean changes from 0.1092 PgC/yr for Q10=1, i.e., without dependency on temperature, to 0.1143 PgC/yr for Q10=2.6, the most strongly temperature-dependent decomposition rate.

This 5% change within the range of possible decomposition rates illustrate the weak dependence of global DOC flux to the ocean on the temperature. We conclude that this is a factor which could be neglected in first approximation.

Table 2: Q10 sensitivity tests for version B, Test 03, and T_{ref} of 293.15 K.

Q10	**Total riverine DOC flux to ocean Pg C year^{-1}**
1.0	0.1092
1.4	0.1124
1.8	0.1138
2.2	0.1143
2.6	0.1145

We tested our model's sensitivity to λ_{Tref} by running a set of simulation with a fixed T_{ref} of 293.15 K using model variant B, f_0 of 0.1% and a Q10 of 2.2. Table 3 shows the yearly total riverine DOC reaching the ocean for a range of λ_{Tref} values. The effect of changed decomposition rate on total flux is significant, with factor of two difference between the slowly and quickly decomposing matter. For the fast decomposition rates of several days to weeks, the response curve is flattens, while for the decomposition rates close to a year the decomposition rate has a much stronger effect on the total flux. We conclude that the parameter λ_{Tref}, or decomposition rate during water transport, has a strong impact on the total riverine carbon flux to the ocean.

Table 3: λ_{Tref} sensitivity tests

λ_{Tref}, **day^{-1}**	**Global DOC flux to ocean, PgC yr^{-1}**
0.0	0.1957
0.004	0.1697
0.008	0.1582
0.046	0.1143
0.08	0.0971
0.172	0.0800

3.2 Effect of spatial resolution

When testing the approach of attributing the water soluble carbon amount mixed to the river flow as a volumetric quantity, the spatial resolution plays a significant role. In the process of upscaling the HD river flow to T63 grid of Yasso soil carbon pools, the river discharge is distributed very coarsely on the spatial grid leading to incorrect peak volumes and seasonality. This problem is amplified when two different rivers within a basin flow close together.

The interpolation of carbon parameters to 0.5° grid introduces numerical differences but in compensation gives a better representation of hydrological properties (rate and direction of river flow) on the HD grid. This effect can be seen when comparing the discharge simulated by the model and the associated simulated carbon flux in different river basins against in-situ observations. The comparatively higher resolution of HD model grid however effects the C flux values only for individual river basins (which fulfills the scope of the present study). The global carbon balance for this process is closed independent on whether the HD grid is similar or different to the JSBACH grid.

3.3 Model sensitivity based on removed soil carbon fraction

The fraction of soil carbon contributing to the riverine carbon flux per day is tested for a range of values and compared to observations. f_0 values of 0.1% and 1% per day are used as a starting point for the sensitivity tests. Since JSBACH and the HD model are spun-up for a long time leading to a carbon as well as hydrological equilibrium, the variation in the input soil carbon fraction is robust and proportional to the riverine carbon flow into the ocean.

4 Results and discussion

The sensitivity studies are focused on evaluating the riverine carbon transport scheme spatially to understand the global patterns along with the DOC seasonality at river mouths for individual river basins.

4.1 Spatial pattern or large scale global distribution of model derived DOC flux

The global distribution of total water soluble carbon is shown in Figure 2 for the Test 01 simulation as detailed in Table 1. The global riverine network on HD grid shows a representative distribution of carbon transported via the hydrological basins. As seen in the figures, the amount of transported carbon is proportional to the river discharge, i.e., the higher the runoff, the higher the amount of carbon transported (the Amazon basin and other large basins show the highest values of transported carbon at their outlet points). Table 4 shows observations of the DOC flux into the ocean for a range of major rivers from *Coynel et. al.* [2005] and *Raymond et. al.* [2007]. In comparison to the two major rivers discussed below, Lena and Amazon, simulated fluxes are about 6.3 and 19 TgC yr^{-1}, respectively. For the Amazon, the simulated value is about half the value given in the Table 4, however, observations also differ in the range of a factor of 2. For the Lena, the simulated total DOC flux is close to observations.

Table 4: DOC fluxes from large tropical and Arctic rivers [*Coynel et. al.*, 2005; *Raymond et. al.*, 2007].

River	**DOC flux to ocean, TgC yr^{-1}**
Amazon	37.6
Congo	12.4
Nile	0.7
Lena	5.83
Ob	3.05
Mackenzie	1.4

4.2 Seasonality of DOC flux for major rivers

We analysed the seasonality for our riverine DOC transport scheme for various river basins. We use Arctic and tropical river basins as test cases as their distinctive characteristics allow us to evaluate the sensitivity of our model to river discharge, topography and soil characteristics (geology, temperature, vegetation). The following sections describe the simulated seasonality of the riverine DOC transport for various river basins.

4.2.1 Arctic rivers

Figure 3 shows the seasonality plot of river discharge and riverine carbon flux for Arctic rivers for model version A (leaching from water soluble pools only) for Test 01 simulation as detailed in Table 1. Simulated river discharge has a strong maximum in June, in line with observations that show a distinct runoff peak in June due to snowmelt and river ice break-up [*Winkelbauer et. al.*, 2022]. The low discharge in winter time is also in line with observations as precipitation is accumulated as snow on the surface in this period. The discharge variance in Arctic rivers is mainly explained by the size of the river's watershed; the Lena (2.46 Mill. km^2) and Ob (2.97 Mill. km^2) rivers' watersheds being largest in extent and hence having the highest discharge while the Mackenzie (1.81 Mill. km^2) and Kolyma (0.64 Mill. km^2) rivers have the smallest watersheds and hence lowest discharges. For the Mackenzie, the precipitation is also noticeably lower than for the two large Siberian catchments [*Arpe et. al.*, 2005]. The DOC transport flux follows the discharge as expected from the model parameterisation, Eq. 3.

Similarly, Figure 4 shows the seasonality plot for Arctic rivers for model version B (leaching from all AWEN pools) for Test 01 simulation. In comparison with the Figure 3, the amount of carbon leached out of the soil is an order of magnitude greater. This is expected as the water soluble pool is only a small fraction of the total soil carbon pool. The DOC flux is proportional to the river discharge and to the available carbon pool, therefore the results shown in the two aforementioned Figures are almost (but not exactly) a linear scaling of one another. Except for this linear scaling with the available carbon, there is no substantial dissimilarity due to different carbon pools being accounted for.

Figure 5 shows the seasonality plot (river discharge and riverine carbon flux) for the Lena river for model version A (leaching from water soluble pools only) for all the simulations detailed in Table 1. As expected, the DOC flux strongly rises with an increase in the carbon fraction leached from 0.1% (Test 01-03) to 1.0% (Test 04-06). The increase is almost proportional, implying a linear scaling with f_0. The change in the turnover time, λ, shows more non-linear behavior. For example, while the DOC peak in the Test 01 coincides with the peak in river discharge, with a stronger decomposition rate the maximum DOC is seen as an earlier month in Test 06. This earlier peak is more in line with the observations as one could see on Figure 6 that shows a comparison of carbon flux for Lena river in comparison to observations [*Raymond et. al.*, 2007]. Test 06 (with defined f_0, λ values) in Table 1 presents a best fit for the Lena river carbon flux simulation. The DOC flux in the model is also substantial in October-December, which is not in line with observations. It might be overestimated due to soil carbon accumulated by the end of the growth period being leached in the model, while this carbon in reality might be frozen and not accessible for leaching.

4.2.2 Tropical rivers

Figure 7 shows a seasonality plot (river discharge and riverine carbon flux) for tropical rivers for model version A (leaching from water soluble pools only) for Test 01 simulation as detailed in Table 1. For the Amazon, Nile, and Xingu rivers, the DOC flux is proportional to the river discharge. For the Congo river the dependence is less linear as the river carries much more DOC in relation to its discharge compared to the previous rivers. Figure 8 shows seasonality a plot (river discharge and riverine carbon flux) for Amazon river for model version A (leaching from water soluble pools only) for all simulations as detailed in Table 1. The DOC flux is proportional to f_0 and λ values, similarly to the Arctic rivers. To compare DOC seasonality with observations, Figure 9 shows a comparison of carbon flux for Amazon river in comparison to observations [*Lauerwald et. al.*, 2017; *Moreira-Turcq et. al.*, 2003]. Test 05 (with defined f_0, λ values) in Table 1 present a best fit for the Amazon river carbon flux simulation. The DOC peak is simulated a month earlier than in the observations, and the model underestimates the carbon transport during the period of low discharge (November to March). This indicates that other processes are important for tropical river DOC transport, especially during the dry season. Since the optimal parameter for the Amazon (λ=0.046) differs from the parameter for the Lena (λ=0.172), we conclude that the model requires regional tuning for some parameters. This could be a consequence of current model assumptions, but also of different seasonality of river discharges in the Arctic and in the tropics. The seasonal variability of the carbon flux for the Congo on Figure 7 is much more pronounced than that of the discharge (in comparison to other rivers), which may indicate that for this catchment the transport of DOC is much more sensitive to changes in the runoff seasonality than in other areas [*Kurek et al.*, 2022]. Note that *Coynel et. al.* [2005] state that the seasonal patterns of DOC show clockwise hysteresis in relation to river discharges, with maximum levels recorded 2 to 4 months before peak flows.

4.3 Limitations of this study

One limitation of this study and our model setup in general is that we use a generic global carbon scaling fraction (based on *Li et. al.* [2017]). The carbon scaling fraction influences the quantity of water soluble carbon available for riverine transport. Ideally, the carbon scaling fraction should be varied between river basins (for example between Arctic or tropical basins), so that the specific characteristics of the basin such as soil carbon properties, topography, vegetation and river discharge can be taken into account; either by the processed based modelling of these factors or by fitting to seasonal observations of DOC for each basin individually or for each class of basins with similar characteristics.

A second limitation of the current study is that it uses the standalone version of JSBACH3 coupled with the HD model to run the riverine DOC transport model; hence our results lack any feedback from the atmospheric state due to the removed land carbon and any feedback from ocean from the influx of riverine DOC into the ocean model.

Additionally to the above, the use of surface runoff as an exclusive carrier for the soil carbon leaching ignores the possible influence of subsurface drainage in the overall riverine DOC. In the current model study, the subsurface drainage C flux is found to be insignificant in comparison to the surface runoff C flux, however, a more inclusive soil scheme as well as constraining model runs with a different forcing data could also influence the overall effect of subsurface C flux component for riverine DOC.

5 Conclusions

In this study we have shown that we are able to model riverine DOC production, transport and decay within JSBACH by combining a simple set of components with a data based tuning. Our study has shown that a key element to correctly modelling the seasonality of riverine DOC flux is scaling the DOC leaching from the soil model according to the surface runoff from the soil hydrology model. However, we have been unable to find a single tuning of the rate of DOC leaching that is able to match observations for both the tropical and Arctic regions - the best fit to observations for the Arctic produces poor results for the Tropics and visa versa. We conclude our model can be used to model riverine DOC flux in one of these regions (with the correct tuning) when the limitation that it gives poor results in the other region is taken into account. We also found that the model results are insensitive to values of the Q10 parameter which allows it to be neglected it in model simulations.

The current study provides an opportunity to link to the coupled ocean model where a Dissolved Inorganic Carbon (DIC) component via soil weathering is being developed as a part of HAMOCC model. In addition, the lateral DOC transport within the HD model has been used to develop a framework for the transport of biogeochemical tracers (such as used by *Simon et. al.* [2023]) that builds up on the most recent version of the HD model [*Hagemann et. al.*, 2020].

6 Model code availability

The MPI-ESM code version that includes the DOC scheme detailed in this document is stored in a branch in the MPI-ESM git repository on the MPI-ESM git server (`git.mpimet.mpg.de`). The specific version used is commit:

`0637315099c4acb952c771281ac9a3b30a122b00`

on the branch `mpiesm-landveg_tcr_doc`. The code is available from the Max Planck Society's Edmond repository (edmond.mpg.de) under the MPI-M Software Licence Agreement; the corresponding entry in the repository can be accessed via the DOI: 10.17617/3.SQOWKV.

7 Acknowledgements

SG and TR are funded by the German Federal Ministry of Education and Research (BMBF) project PalMod. VB research is supported by the European Research Council under the European Union's Horizon 2020 research and innovation program as part of the Q-Arctic project (Grant agreement No 951288). Furthermore, the research was supported by the German Research Foundation as part of the CLICCS Clusters of Excellence (DFG EXC 2037). The authors would like to thank Veronika Gayler for her assistance in understanding and modifying JSBACH 3 for this work. The authors are also grateful to Dr. Tobias Stacke for his useful and constructive comments.

References

Amon, R., M., W., and Benner R., (1996), Bacterial utilization of different size classes of dissolved organic matter. *Limnol. and Oceanogr. 41*, 41–51, doi:10.4319/lo.1996.41.1.0041.

Arpe, K., Hagemann, S., Jacob, D., and Roeckner, E. (2005), The realism of the ECHAM5 models to simulate the hydrological cycle in the Arctic and North European area, *Nord. Hydrol.*, *36*, 349–367, doi:10.2166/nh.2005.0027

Battin, T. J., S. Luyssaert, L. A. Kaplan, A. K. Aufdenkampe, A. Richter, and L. J. Tranvik (2009), The boundless carbon cycle. *Nat. Geosci.* , *2*, 598–600, doi:10.1038/ngeo618

Canadell, J. G., Monteiro, P. M. S., Costa, M. H., Cotrim da Cunha, L., Cox, P. M., Eliseev, A. V., Henson, S., Ishii, M., Jaccard, S., Koven, C., Lohila, A., Patra, P. K., Piao, S., Rogelj, J., Syampungani, S., Zaehle, S., and Zickfeld, K. (2021): Global Carbon and other Biogeochemical Cycles and Feedbacks. In Climate Change 2021: The Physical Science Basis. Contribution of Working Group I to the Sixth Assessment Report of the Intergovernmental Panel on Climate Change [Masson-Delmotte, V., Zhai, P., Pirani, A., Connors, S.L., Péan, C., Berger, S., Caud, N., Chen, Y., Goldfarb, L., Gomis, M.I., Huang, M., Leitzell, K., Lonnoy, E., Matthews, J.B.R., Maycock, T.K., Waterfield, T., Yelekçi, O., Yu, R., and Zhou B. (eds.)]. *Cambridge University Press, pp. 673–816,* doi:10.1017/9781009157896.007.

Cole, J. J., Prairie, Y. T., Caraco, N. F., McDowell, W. H., Tranvik, L. J., Striegl, R. G., Duarte, C. M., Kortelainen, P., Downing, J. A., Middelburg J. J., and Melack J. (2007), Plumbing the Global Carbon Cycle: Integrating Inland Waters into the Terrestrial Carbon Budget. *Ecosystems*, *10*, 172–185, doi:10.1007/s10021-006-9013-8

Compo, G. P., Whitaker, J. S., Sardeshmukh, P. D., Matsui, N., Allan, R. J., Yin, X., Gleason, B. E., Vose, R. S., Rutledge, G., Bessemoulin, P., Brönnimann, S., Brunet, M., Crouthamel, R. I., Grant, A. N., Groisman, P. Y., Jones, P. D., Kruk, M. C., Kruger, A. C., Marshall, G. J., Maugeri, M., Mok, H. Y., Nordli, Ø., Ross, T. F., Trigo, R. M., Wang, X. L., Woodruff, S. D. and Worley, S. J. (2011), The Twentieth Century Reanalysis Project., *Q.J.R. Meteorol. Soc.*, *137*, 1–28, doi:10.1002/qj.776

Cory, R. M., Ward, C. P., Crump, B. C., and Kling, G. W. (2014), Sun- light controls water column processing of carbon in arctic fresh waters. *Science*, *345*, 925–928, doi:10.1126/science.1253119.

Coynel, A., Seyler, P., Etcheber, H., Meybeck, M., and Orange, D. (2005), Spatial and seasonal dynamics of total suspended sediment and organic carbon species in the Congo River. *Global Biogeochem. Cy.*, *19*, doi:10.1029/2004GB002335.

Dirmeyer, P. A., Gao, X., Zhao, M., Guo, Z., Oki, T. and Hanasaki, N. (2006), GSWP-2: Multimodel Analysis and Implications for Our Perception of the Land Surface, *B. Am. Meteorol. Soc.*, *87(10)*, 1381—98.

Ekici, A., Beer, C., Hagemann, S., Boike, J., Langer, M., and Hauck, C. (2014), Simulating high-latitude permafrost regions by the JSBACH terrestrial ecosystem model. *Geosci. Model Dev.*, *7*, 631–647, doi:10.5194/gmd-7-631-2014.

Giorgetta, M. A., Jungclaus, J., Reick, C. H., Legutke, S., Bader, J., Böttinger, M., Brovkin, V., Crueger, T., Esch, M., Fieg, K., Glushak, K., Gayler, V., Haak, H., Hollweg, H.-D., Ilyina, T., Kinne, S., Kornblueh, L., Matei, D., Mauritsen, T., Mikolajewicz, U., Mueller, W., Notz, D., Pithan, F., Raddatz, T., Rast, S., Redler, R., Roeckner, E., Schmidt, H., Schnur, R., Segschneider, J., Six, K. D., Stockhause, M., Timmreck, C., Wegner, J., Widmann, H., Wieners, K.-H., Claussen, M., Marotzke, J., and Stevens, B, (2013), Climate and carbon cycle changes from 1850 to 2100 in MPI-ESM simulations for the Coupled Model Intercomparison Project phase 5. *J. Adv. Model. Earth Sy.*, *5*, 572–597, doi:10.1002/jame.20038.

Goll, D. S., Brovkin, V., Liski, J., Raddatz, T., Thum, T., and Todd-Brown, K. E. O, (2015), Strong dependence of CO2 emissions from anthropogenic land cover change on initial land cover and soil carbon parametrization. *Global Biogeochem. Cy.*, *29*, 1511–1523, doi:10.1002/2014GB004988.

Hagemann, S. and Dümenil, L. (1998), A parametrization of the lateral waterflow for the global scale. *Clim. Dynam*, *14*, 17–31, doi:10.1007/s003820050205.

Hagemann, S. and Dümenil-Gates, L. (2001), Validation of the hydrological cycle of ECMWF and NCEP reanalyses using the MPI hydrological discharge model. *J. Geophys. Res.-Atm.*, *106*, 1503–1510, doi:10.1029/2000JD900568.

Hagemann, S., and Stacke, T. (2015), Impact of the soil hydrology scheme on simulated soil moisture memory. *Clim. Dyn.*, *44*, 1731–1750, doi:10.1007/s00382-014-2221-6.

Hagemann, S., Stacke, T., and Ho-Hagemann, H.T.M. (2020), High Resolution Discharge Simulations Over Europe and the Baltic Sea Catchment, *Front. Earth Sci.*, *8*, doi:10.3389/feart.2020.00012

Hansell, D. a., Kadko, D., and Bates, N. R. (2004), Degradation of terrigenous dissolved organic carbon in the western Arctic Ocean. *Science*, *304(5672)*, 858–861, doi:10.1126/science.1096175.

Jackson, R. B., Banner, J. L., Jobbágy, E. G., Pockman, W. T., and Wall, D. H. (2002), Ecosystem carbon loss with woody invasion of grasslands. *Nature*, *418*, 623–626, doi:10.1038/nature00910.

Kim, H. (2017), Global Soil Wetness Project Phase 3 Atmospheric Boundary Conditions (Experiment 1) [Data set], Data Integration and Analysis System (DIAS), doi:10.20783/DIAS.501.

Kurek, M. R., Stubbins, A., Drake, T. W., Dittmar, T., Moura, J. M. S., Holmes, R. M., Osterholz, H., Six, J., Wabakanghanzi, J. N., Dinga, B., Mitsuya, M., and Spencer, R. G. M. (2022), Organic Molecular Signatures of the Congo River and Comparison to the Amazon, *Global Biogeochem. Cy.*, *36*, doi:10.1029/2022GB007301.

Lacroix, F., Ilyina, T., Mathis, M., Laruelle, G. G., and Regnier, P. (2021), Historical increases in land-derived nutrient inputs may alleviate effects of a changing physical climate on the oceanic carbon cycle. *Glob. Change Biol.*, *27*, 5491–5513, doi:10.1111/gcb.15822.

Lauerwald, R., Regnier, P., Camino-Serrano, M., Guenet, B., Guimberteau, M., Ducharne, A., Polcher, J., and Ciais, P. (2017), ORCHILEAK (revision 3875): a new model branch to simulate carbon transfers along the terrestrial–aquatic continuum of the Amazon basin, *Geosci. Model Dev.*, *10*, 3821–3859, doi:10.5194/gmd-10-3821-2017.

Li, M., Peng, C., Wang, M., Xue, W., Zhang, K., Wang, K., Shi, G. and Zhu, Q. (2017), The carbon flux of global rivers: A re-evaluation of amount and spatial patterns. *Ecol. Indic.*, *80*, 40–51, doi:10.1016/j.ecolind.2017.04.049.

Li, M., Peng, C., Zhou, X., Yang, Y., Guo, Y., Shi, G., and Zhu, Q., (2019), Modeling Global Riverine DOC Flux Dynamics From 1951 to 2015. *J. Adv. Model. Earth Sy.*, *11*, 514–530, doi:10.1029/2018MS001363.

Mauritsen, T., Bader, J., Becker, T., Behrens, J., Bittner, M., Brokopf, R., Brovkin, V., Claussen, M., Crueger, T., Esch, M., Fast, I., Fiedler, S., Fläschner, D., Gayler, V., Giorgetta, M., , Goll, Daniel S., Haak, H., Hagemann, S., Hedemann, C., Hohenegger, C., Ilyina, T., Jahns, T., Jimenéz-de-la-Cuesta, D., Jungclaus, J., Kleinen, T., Kloster, S., Kracher, D., Kinne, S., Kleberg, D., Lasslop, G., Kornblueh, L., Marotzke, J., Matei, D., Meraner, K., Mikolajewicz, U., Modali, K., Möbis, B., Müller, W. A., Nabel, J. E. M. S. , Nam, C. C. W. , Notz, D. , Nyawira, S.-S., Paulsen, H., Peters, K., Pincus, R., Pohlmann, H., Pongratz, J., Popp, M., Raddatz, T. J. , Rast, S., Redler, R., Reick, C. H., Rohrschneider, T., Schemann, V., Schmidt, H., Schnur, R., Schulzweida, U., Six, K. D., Stein, L., Stemmler, I., Stevens, B., von Storch, J.-S. , Tian, F. , Voigt, A., Vrese, P., Wieners, K.-H., Wilkenskjeld, S., Winkler, A., and Roeckner, E. (2019), Developments in the MPI-M Earth System Model version 1.2 (MPI-ESM1.2) and its response to increasing CO2. *J. Adv. Model. Earth Sy.*, *11*, 998–1038, doi:10.1029/2018MS001400.

Meybeck M. (1993), Riverine transport of atmospheric carbon - sources, global typology and budget, *Water Air Soil Pollut., 70 (1- 4)*, 443–463.

Moreira-Turcq, P., Seyler, P., Guyot, J. L., and Etcheber, H. (2003), Exportation of organic carbon from the Amazon River and its main tributaries. *Hydrol. Process.*, *17,* 1329–1344, doi:10.1002/hyp.1287.

Raymond, P. A., McClelland, J. W., Holmes, R. M., Zhulidov, A. V., Mull, K., Peterson, B. J., Striegl, R. G., Aiken, G. R., and Gurtovaya, T. Y. (2007), Flux and age of dissolved organic carbon exported to the Arctic Ocean: A carbon isotopic study of the five largest arctic rivers, *Global Biogeochem. Cy.*, *21*, doi:10.1029/2007GB002934.

Reick, C. H., Raddatz, T., Brovkin, V., and Gayler, V. (2013), Representation of natural and anthropogenic land cover change in MPI-ESM, *J. Adv. Model. Earth Sy. 5,* 459–482, doi:10.1002/jame.20022.

Reick, C. H., Gayler, V., Goll, D., Hagemann, S., Heidkamp, M., Nabel, J. E. M. S., Raddatz, T., Roeckner, E., Schnur R., Wilkenskjeld, S. (2021), JSBACH 3 - The land component of the MPI Earth System Model: documentation of version 3.2. Hamburg, *MPI für Meteorologie*, doi:10.17617/2.3279802.

Schlesinger, W. H., and Melack, J. M. (1981), Transport of organic carbon in the world's rivers, *Tellus, 33,* 172–187.

Schneck, R., Reick, C. H., and Raddatz, T. (2013), Land contribution to natural CO2 variability on time scales of centuries, *J. Adv. Model. Earth Sy. 5,* 354–365, doi:10.1002/jame.20029.

Simon, P., M. Ramacher, S. Hagemann, H. Joerss, J. Bieser (2023), POPE: a Global Gridded Emission Inventory for PFOA 1950-2020. *Environ. Sci. Technol.* (submitted)

Taylor, K. E., Stouffer, R. J., and Meehl, G. A. (2012), An Overview of CMIP5 and the Experiment Design, *B. Am. Meteorol. Soc. 93,* 485–498, doi:10.1175/BAMS-D-11-00094.1.

Textor, S., R., Wickland, K., P., Podgorski, D., C., Johnston, S., E., and Spencer, R., G., M., (2019), Dissolved Organic Carbon Turnover in Permafrost-Influenced Watersheds of Interior Alaska: Molecular Insights and the Priming Effect, *Front. Earth Sci. 7,* doi:10.3389/feart.2019.00275.

Thum, T., Raisanen, P. Sevanto, S., Tuomi, M., Reick, C., Vesala, T., Raddatz, T., Aalto, T., Järvinen, H., Altimir, N., Pilegaard, K., Nagy, Z., Rambal, S., and Liski, J. (2011), Soil carbon model alternatives for ECHAM5/JSBACH climate model: Evaluation and impacts on global carbon cycle estimates, *J. Geophys. Res. 116,* doi:10.1029/2010JG001612.

Tian, H., Yang, Q., Najjar, R., G., Ren, W., Friedrichs, M., A., M., Hopkinson, C., S., and Pan, S. (2015), Anthropogenic and climatic influences on carbon fluxes from eastern North America to the Atlantic Ocean: A process-based modeling study, *J. Geophys. Res. 120,* doi:10.1002/2014JG002760.

Tuomi, M., Vanhala, P., Karhu, K., Fritze, H., and Liski, J. (2008), Heterotrophic soil respiration comparison of different models describing its temperature dependence, *Ecol. Model. 211(1-2),* 182–190, doi:10.1016/j.ecolmodel.2007.09.003.

Winkelbauer, S., Mayer, M., Seitner, V., Zsoter, E., Zuo, H., and Haimberger, L. (2022), Diagnostic evaluation of river discharge into the Arctic Ocean and its impact on oceanic volume transports, *Hydrol. Earth Syst. Sci. 26*, 279–304, doi:10.5194/hess-26-279-2022

Yang, D., Robinson, D., Zhao, Y., Estilow, T., and Ye, B. (2003), Streamflow response to seasonal snow cover extent changes in large Siberian watersheds, *J. Geophys. Res.-Atmos. 108,* D18, doi:10.1029/2002jd003149

Yoshimura, K., and Kanamitsu, M. (2008), Dynamical Global Downscaling of Global Reanalysis, *Mon. Weather Rev.*, *136(8)*, 2983–2998

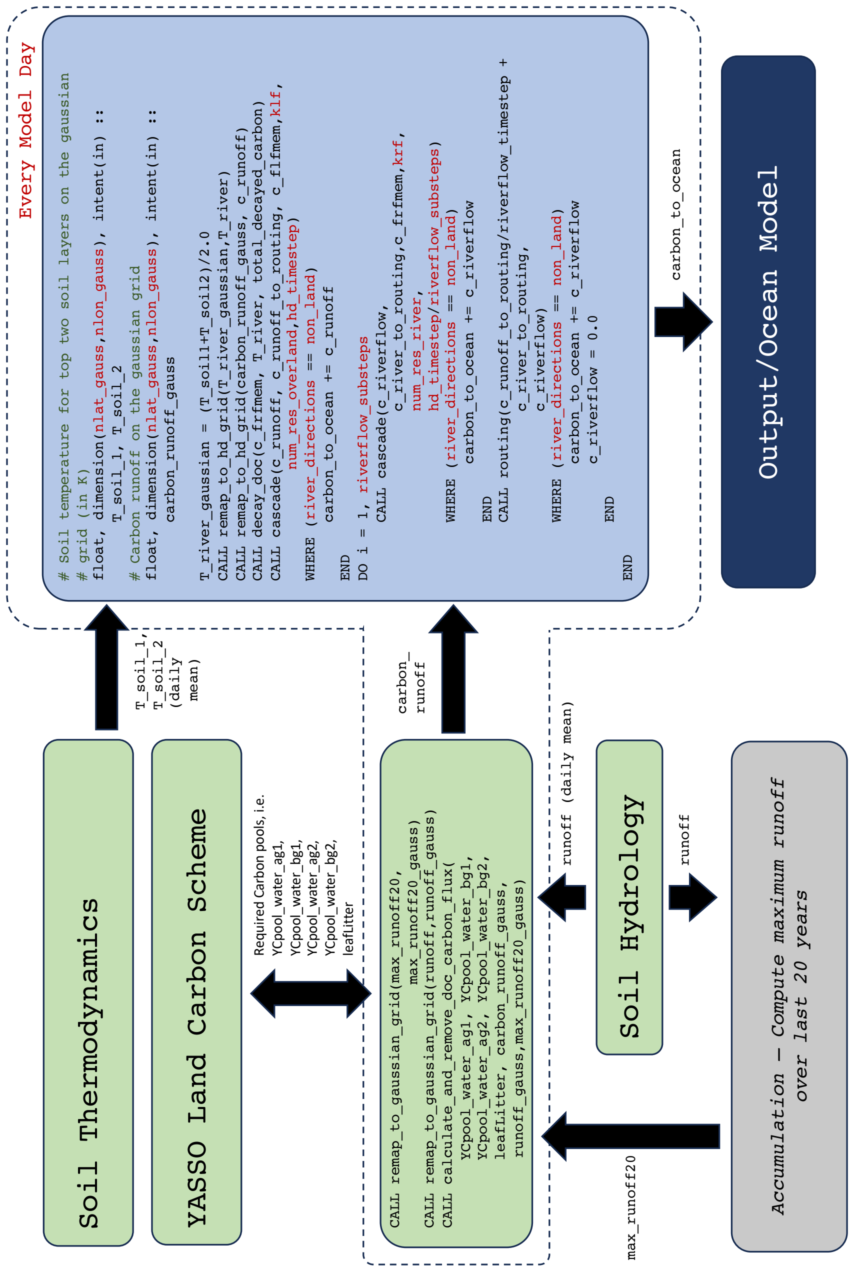

Figure 1: Block diagram showing the principle routines of the DOC scheme and their location in the wider JSBACH3 code. Constants are marked in this red and are assumed to be available wherever they are needed. The handling of input and output is omitted. This page show the overall scheme - subsequent pages give the definitions of required subroutines and constants.

```
SUBROUTINE decay_doc(res_content,T_river,decayed_carbon)

# Riverine DOC reservoir levels
float, dimension(nlat,nlon), intent(inout) :: res_content
# Temperature of the river, 1st and 2nd layer layer soil temperature
# remapped from the gaussian grid is used as a proxy for this
# Units must be K
float, dimension(nlat,nlon), intent(in)    :: T_river
# Amount of riverine DOC release to the atmosphere at this timestep
float, dimension(nlat,nlon), intent(out)   :: decayed_carbon

      decayed_carbon[:,:] = 0
      DO lat = 1,nlat
      DO lon = 1,nlon
            doc_decay_factor =
                  EXP(-1.0*
                      doc_decay_lambda_Tref*
                      doc_decay_Q10**((T_river[lat,lon] -
                                       doc_decay_Tref)/10.0)*
                      hd_timestep)
            DO k = 1, num_res_river[lat,lon]
                  res_content_updated = doc_decay_factor*
                                        res_content[lat,lon,k]
                  decayed_carbon[lat,lon] += res_content[lat,lon,k] –
                                             res_content_updated
                  res_content[lat,lon,k] = res_content_updated
            END
      END
      END

END SUBROUTINE
```

```
SUBROUTINE routing(inflow,outflow)

float, dimension(nlat,nlon), intent(in) :: inflow
float, dimension(nlat,nlon), intent(out) :: outflow

Add content of each cell in inflow to next neighboring downstream to
give output according to a set of river directions
```

```
SUBROUTINE remap_to_gaussian_grid(input,output)

float, dimension(nlat,nlon), intent(in) :: input
float, dimension(nlat_gauss,nlon_gauss), intent(out) :: ouput

Remap input from JSBACH's main gaussian latitude-longitude grid to the
HD model's half degree regular latitude-longitude grid using a
predefined mapping
```

```
SUBROUTINE calculate_and_remove_doc_carbon_flux(
        YCpool_water_ag1, YCpool_water_bg1,
        YCpool_water_ag2, YCpool_water_bg2,
        leafLitter, carbon_runoff,
        runoff,max_runoff20)

# Relevant YASSO carbon pools
float, dimension(nlat_gauss,nlon_gauss), intent(inout) ::
       YCpool_water_ag1, YCpool_water_bg1,
       YCpool_water_ag2, YCpool_water_bg2,
       leafLitter
# Carbon runoff to HD model
float, dimension(nlat_gauss,nlon_gauss), intent(out) ::
       carbon_runoff
# Runoff to HD model and 20-year maximum runoff to HD
# model
float, dimension(nlat_gauss,nlon_gauss), intent(out) ::
       runoff,max_runoff20

       f_leach_runoff = MIN(1.0,
                            runoff/MAX(1.0e-13,
                            max_runoff20))
       carbon_runoff = f_leach_runoff *
                       frac_leafLitter_to_HD *
                       leafLitter
       leafLitter -= carbon_runoff
       carbon_runoff   += (YCpool_water_ag1 +
                           YCpool_water_ag2 +
                           YCpool_water_bg1 +
                           YCpool_water_bg2 )*
                           f_leach_runoff *
                           frac_ws_green_to_HD
       YCpool_water_ag1 -= YCpool_water_ag1 *
                           f_leach_runoff *
                           frac_ws_green_to_HD
       YCpool_water_bg1 -= YCpool_water_bg1 *
                           f_leach_runoff *
                           frac_ws_green_to_HD
       YCpool_water_ag2 -= YCpool_water_ag2 *
                           f_leach_runoff *
                           frac_ws_green_to_HD
       YCpool_water_bg2 -= YCpool_water_bg2 *
                           f_leach_runoff *
                           frac_ws_green_to_HD

END SUBROUTINE
```

Figure 1: (Continued) Block diagram showing the principle routines of the DOC scheme and their location in the wider JSBACH3 code. Constants are marked in this red and are assumed to be available wherever they are needed. The handling of input and output is omitted. This page gives the definitions of required subroutines.

```
# This routine is part of the main HD module but also used by the
# riverine DOC code
SUBROUTINE cascade(inflow,outflow,reservoirs,retention_coefficients,
                   reservoirs_nums,steplen)

# DOC reservoir levels
float, dimension(nlat,nlon), intent(inout) :: reservoirs
# Retention coefficients
float, dimension(nlat,nlon), intent(in)    :: retention_coefficients
# Number of reservoirs
integer, dimension(nlat,nlon), intent(in)  :: reservoirs_nums
# Carbon flux in
float, dimension(nlat,nlon), intent(in)    :: inflow
# Carbon flux out
float, dimension(nlat,nlon), intent(out)   :: outflow
# Cascade step length
float :: steplen

      DO i=1,nlat
             DO j=1,nlon
                    flow = inflow(i,j)
                    DO n = 1,reservoir_nums(i,j)
                           new_reservoir_value = reservoirs(i,j,n) + flow
                           amod = retention_coefficients(i,j)/steplen
                           flow = new_reservoir_value/
                                         (amod + 1.0)
                           reservoirs(i,j,n) = new_reservoir_value – flow
                    END
                    outflow(i,j) = flow
             END
      END

END SUBROUTINE
```

```
SUBROUTINE remap_to_hd_grid(input,output)

float, dimension(nlat_gauss,nlon_gauss), intent(in) :: input
float, dimension(nlat,nlon), intent(out) :: output

Remap input from the HD model's half degree regular latitude-longitude
grid to JSBACH's main gaussian latitude-longitude grid using a predefined
mapping
```

```
# Constants

# Scalar constants:
# Read from a configurations settings file or
# hard-coded
# Grid dimensions of main JSBACH gaussian grid
integer :: nlat_gauss, nlon_gauss
# Grid dimension of HD model half-degree regular
# latitude-longitude grid
integer :: nlat, nlon
# HD model direction code for an internal sink point or
# coastal ocean cell
type(river_direction) :: non_land
# Number of substep to use for the carbon riverflow
# cascade
integer :: riverflow_substeps = 5
# DOC decay constant at a refence temperature
float :: doc_decay_lambda_Tref
# Refence temperature for DOC decay constant
float :: doc_decay_Tref
# Q10 value for DOC decay
float :: doc_decay_Q10
# Length of HD model timestep in seconds
float :: hd_timestep
# Fraction of leaf litter carbon pool to add to DOC
# flux at each model timestep
float :: frac_leafLitter_to_HD
# Fraction of water soluble green carbon pool to leach
# to carbon runoff each timestep
float :: frac_ws_green_to_HD

# Constant arrays:
# Read from input netcdf files – all part of the main HD
# module but also used by the riverine DOC scheme
# River routings
type(river_direction), dimension(nlat,nlon) ::
      river_directions
# River flow retention coefficients
float, dimension(nlat,nlon) :: krf
# Overland flow retention coefficients
float, dimension(nlat,nlon) :: klf
# Number of river flow sub-reservoirs per grid box
# Set to 1 for lakes, 5 elsewhere
integer, dimension(nlat,nlon) :: num_res_river
# Number of overland flow sub-reservoirs per grid box
# Set to 1 everywhere
integer, dimension(nlat,nlon) :: num_res_overland
```

Figure 1: (Continued) Block diagram showing the principle routines of the DOC scheme and their location in the wider JSBACH3 code. Constants are marked in this red and are assumed to be available wherever they are needed. The handling of input and output is omitted. This page gives the definitions of required subroutines and constants.

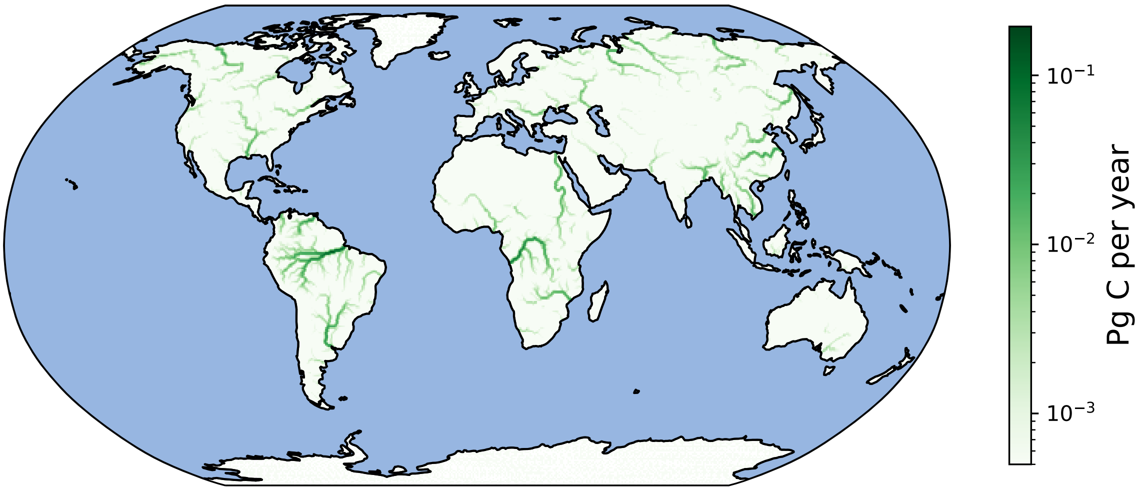

Figure 2: Global distribution of riverine carbon flux, PgC year^{-1}, based on Yasso water soluble carbon pools as simulated by the HD model flow properties. Yasso carbon pools are computed on JSBACH T63 grid, and are used as a primary carbon flux source for deriving the dissoved organic carbon within the global riverine network on a finer HD grid (0.5°)

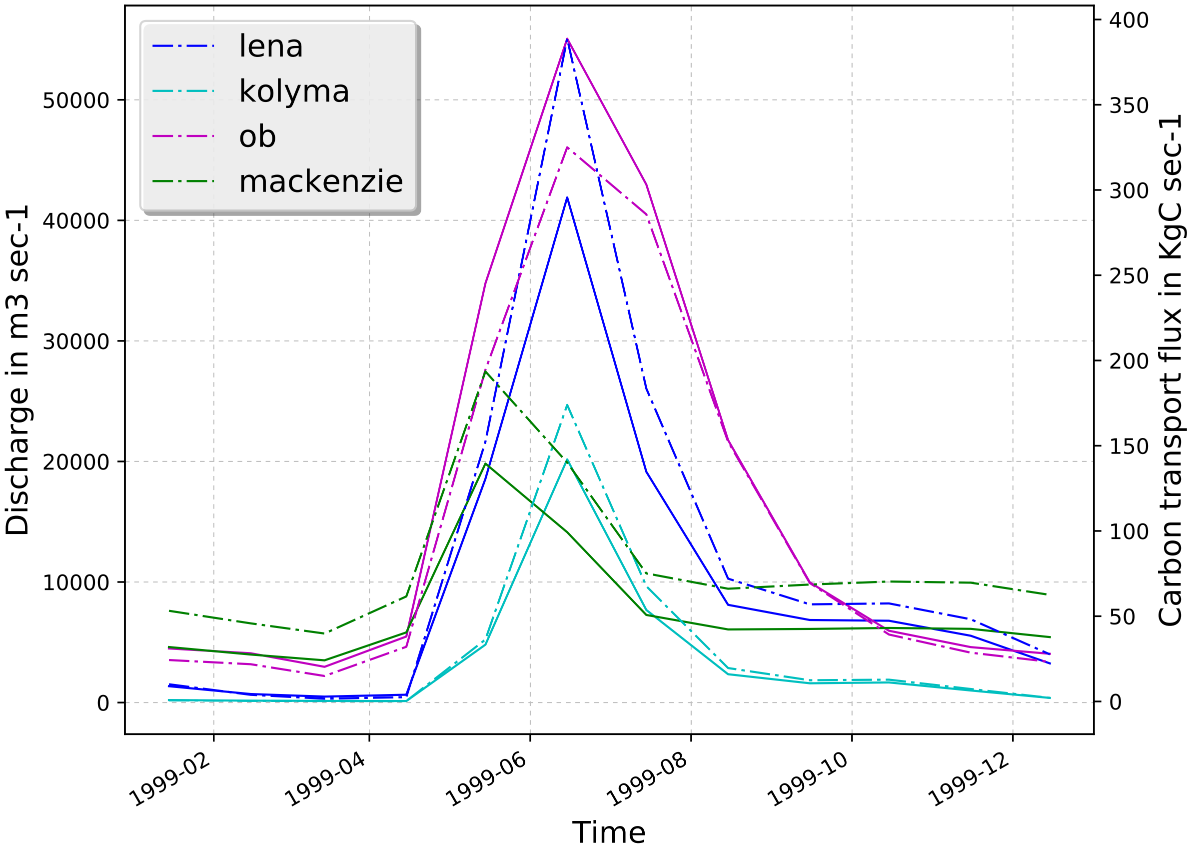

Figure 3: Monthly-averaged seasonal dynamics of carbon fluxes based on Yasso water soluble carbon pools for several Arctic rivers. For each river basin, solid lines shows the river discharge values (corresponding left vertical axis in m^3/s), and the dotted lines represent the seasonality of carbon flux values (corresponding right vertical axis in kgC/s). Results are for the Test 01 experiment with values of f_0= 0.1% and λ_{Tref} = 0.

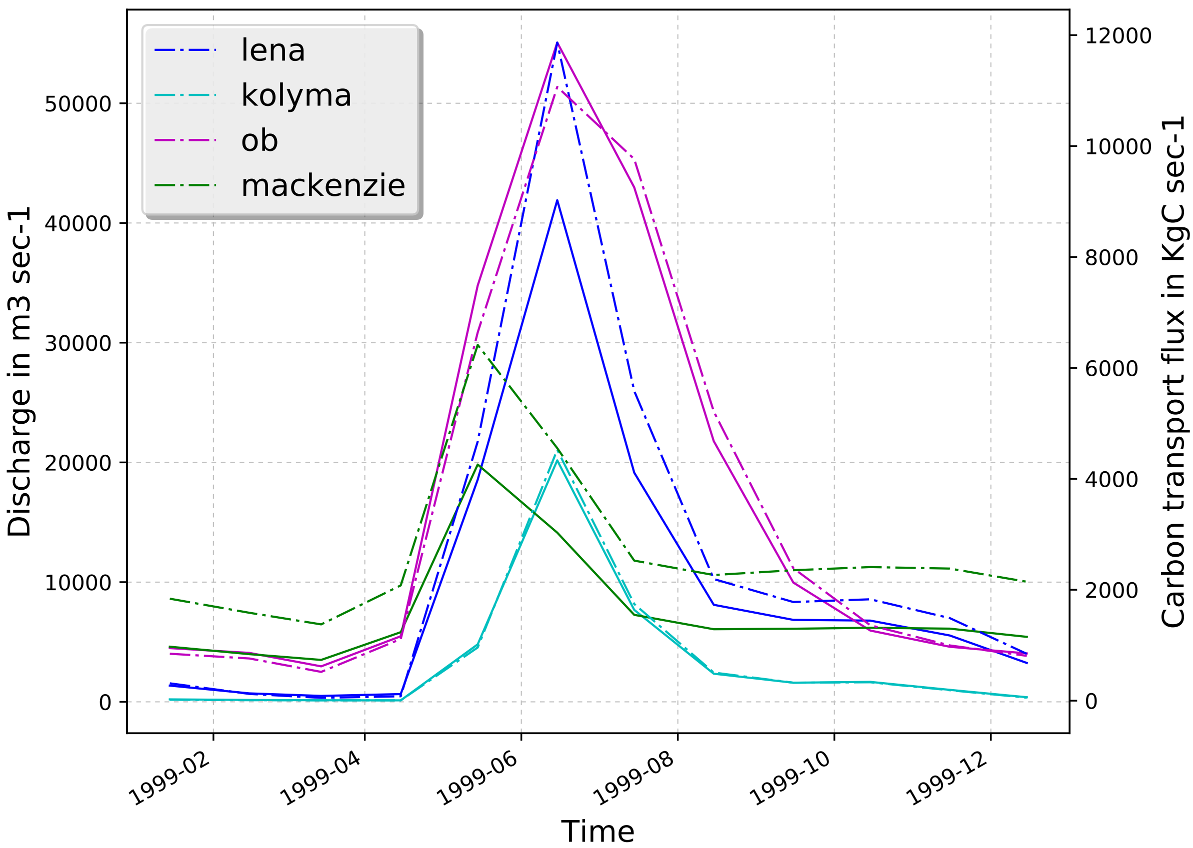

Figure 4: Monthly-averaged seasonal dynamics of carbon fluxes based on total AWEC Yasso pools for several Arctic rivers. For each river basin, solid lines shows the river discharge values (corresponding left vertical axis in m^3/s), and the dotted lines represent the seasonality of carbon flux values (corresponding right vertical axis in kgC/s). Results are for the Test 01 experiment with values of f_0= 0.1% and λ_{Tref} = 0.

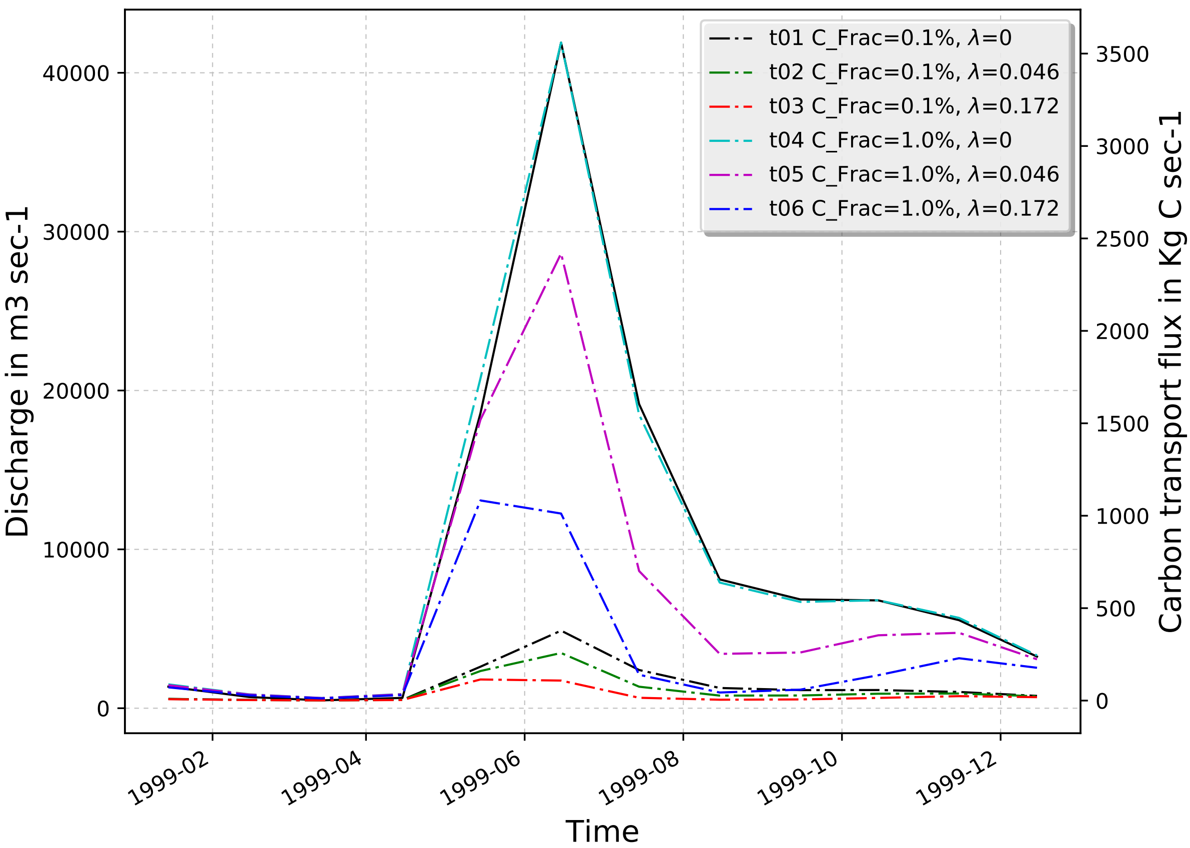

Figure 5: Results of sensitivity simulations for monthly averaged fluxes for Lena river based on Yasso water soluble carbon pools. Solid lines show the river discharge values (corresponding left vertical axis in m^3/s), and the dotted lines represent the seasonality of carbon flux values (corresponding right vertical axis in kgC/s). Test simulations 01 to 06 are with changing values for f_0 (CFrac) and λ_{Tref}.

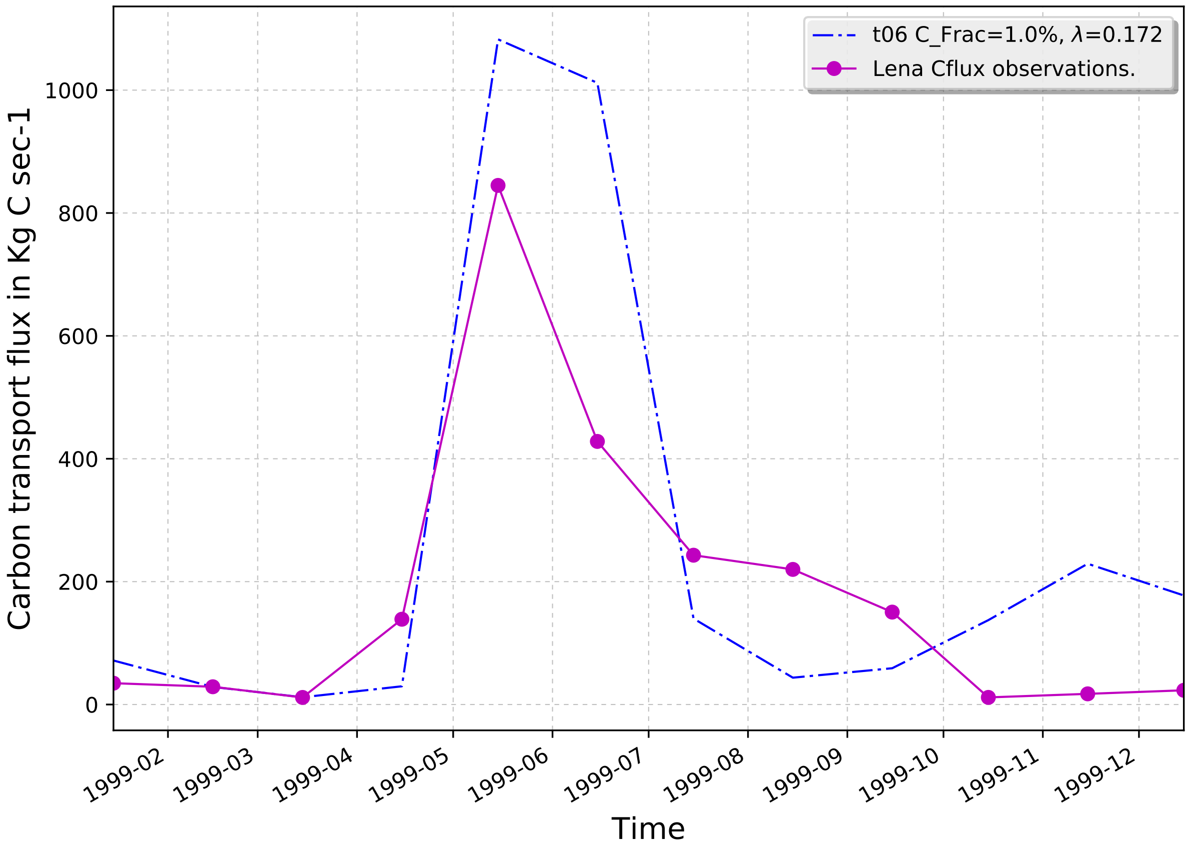

Figure 6: Seasonal carbon flux for the Lena river for Yasso water soluble carbon pools for the best fit (t06) in comparison with in-situ observations [*Raymond et. al.*, 2007]. Magenta solid line corresponds to the observations and blue dotted line corresponds to the best fit test experiment (Test 06) with best fit values of f_0 (CFrac = 1.0 %) and $\lambda_{Tref} = 0.172$.

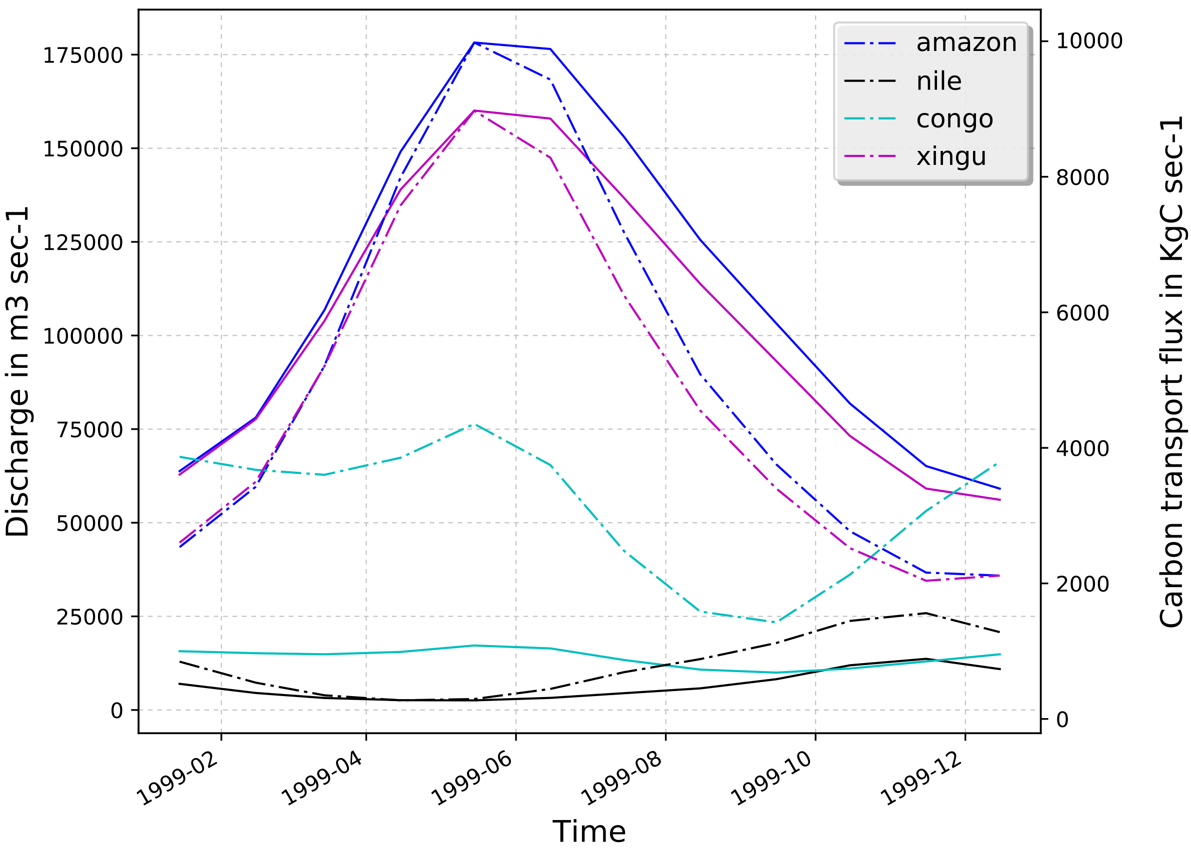

Figure 7: Average seasonal variation of carbon fluxes based on Yasso water soluble carbon pools for selected tropical rivers. For each river basin, solid lines shows the discharge values (corresponding left vertical axis in m^3/s), and the dotted lines represent the seasonality of carbon flux values (corresponding right vertical axis in kgC/s). Results are for the Test 01 experiment with values of f_0= 0.1% and λ_{Tref} = 0.

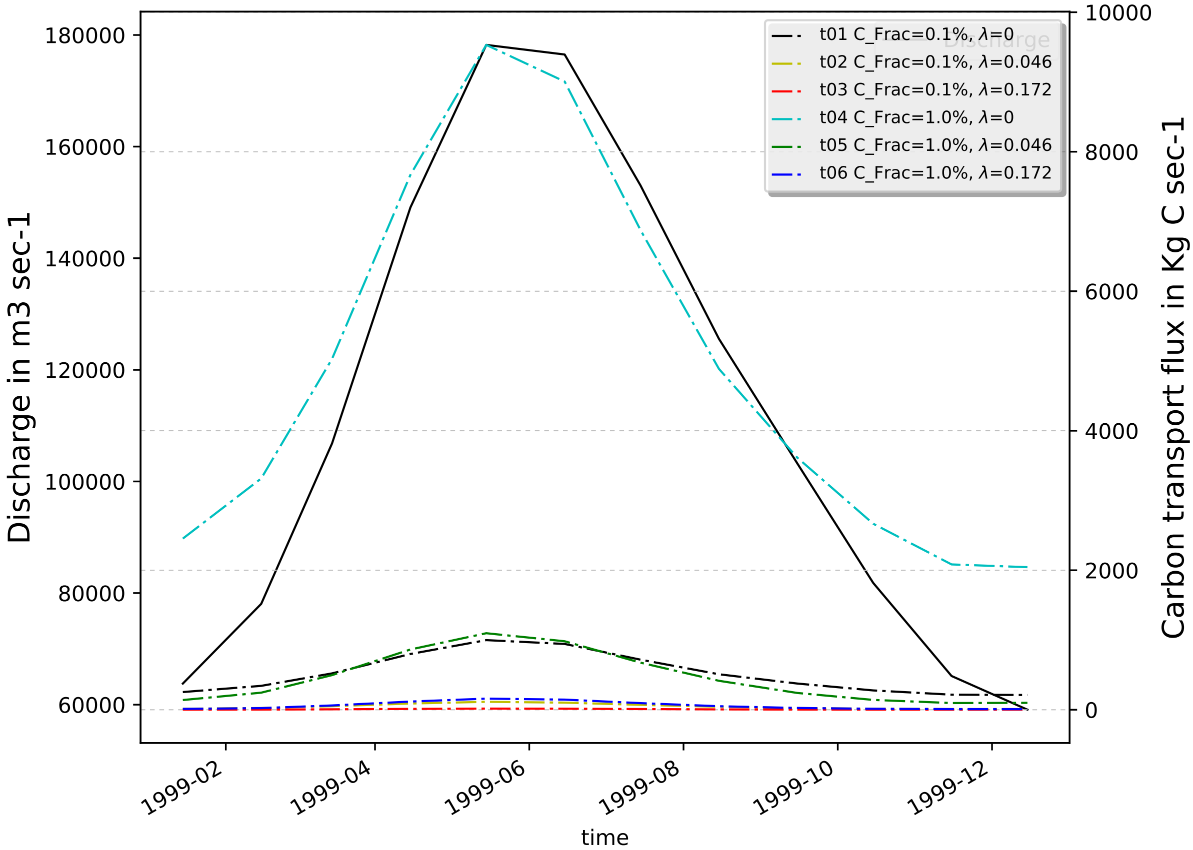

Figure 8: Monthly averaged dynamics of fluxes for Amazon based on Yasso water soluble carbon pools. Solid line shows the river discharge values (corresponding left vertical axis in m^{-3}/s), and the dotted lines represent the seasonality of carbon flux values (corresponding right vertical axis in kgC/s). Various test experiments (Test 01 to Test 06 - here labeled t01 to t06) with changing values for f_0 (CFrac) and λ_{Tref} are shown.

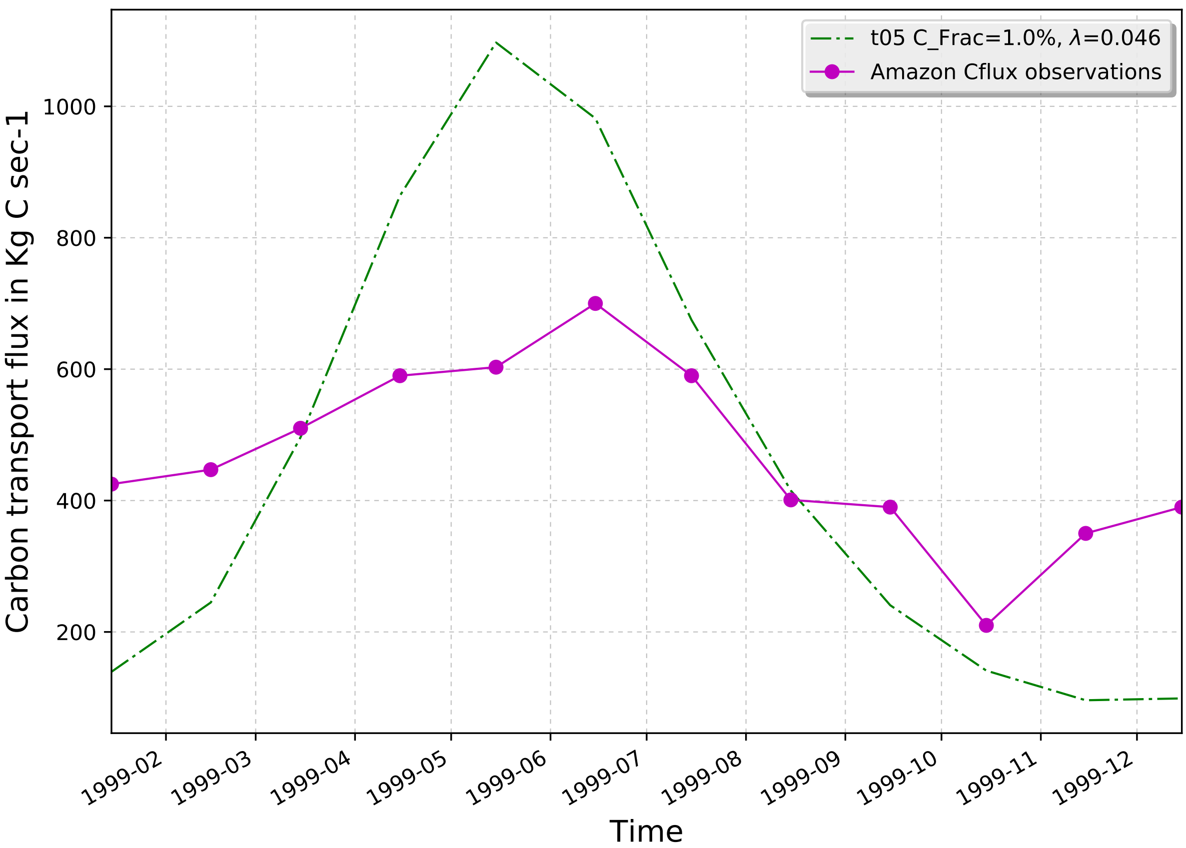

Figure 9: Seasonal carbon flux for the Amazon river for Yasso water soluble carbon pools for the best fit in comparison with in-situ observations [*Lauerwald et. al.*, 2017; *Moreira-Turcq et. al.*, 2003]. Magenta solid line corresponds to the observations and blue dotted line corresponds to the best fit test experiment (Test 05) with best fit values of f_0 (CFrac = 1.0 %) and $\lambda_{Tref} = 0.046$.

Hinweis / Reference

Die gesamten Veröffentlichungen in der Publikationsreihe des MPI-M
„Berichte zur Erdsystemforschung / Reports on Earth System Science“,
ISSN 1614-1199

sind über die Internetseiten des Max-Planck-Instituts für Meteorologie erhältlich:
https://mpimet.mpg.de/forschung/publikationen

All the publications in the series of the MPI -M
„Berichte zur Erdsystemforschung / Reports on Earth System Science“,
ISSN 1614-1199

are available on the website of the Max Planck Institute for Meteorology:
https://mpimet.mpg.de/en/research/publications